# On the Electro-Mechanical Stability of Elastomeric Coaxial Fibers

**D. R. Clarke**
School of Engineering and Applied Sciences,
Harvard University,
Cambridge, MA 02138
e-mail: clarke@seas.harvard.edu

**J. W. Hutchinson**
School of Engineering and Applied Sciences,
Harvard University,
Cambridge, MA 02138-2933
e-mail: jhutchin@fas.harvard.edu

*The stability of cylindrical coaxial fibers made from soft elastomeric materials is studied for electro-static loadings. The general configuration considered is a three-component axisymmetric fiber having a conducting core bonded to a dielectric annulus in turn bonded to an outer conducting annular sheath. A voltage difference between the conducting components is imposed. The stresses and actuated elongation in the perfectly concentric fiber are analyzed, and the critical voltage at which stability of the concentric configuration is lost is determined via solution of the non-axisymmetric bifurcation problem. The role of the geometry and moduli contrasts among the components is revealed, and the sub-class of two-component fibers is also analyzed. The idealized problem of a planar layer with conducting surfaces that is bonded to a stiff substrate on one surface and free on the other exposes the importance of short wavelength surface instability modes.* [DOI: 10.1115/1.4050397]

*Keywords: elasticity, mechanical properties of materials, micromechanics*

## 1 Introduction

The coaxial geometry is an alternative actuator configuration to the parallel plate, planar capacitor that forms the basis for most of dielectric elastomer actuators designs discussed in the electromechanics community [1,2] and the soft-robotics literature [3]. Geometrically, the electrode and dielectric configurations are identical to standard, coaxial cables used for screening electrical signals and for high-frequency transmission lines. Consequently, in contrast to the planar actuator configuration, when a voltage is applied between the inner and outer electrodes, the electric field in the dielectric is not spatially uniform but varies radially. Because of the high modulus of the materials typically used in coaxial cables, such as polyethylene and copper, the electro-static forces produced are insufficient to produce appreciable actuation. However, when a soft elastomer (shear modulus $\sim$ 10–200 kPa compared with 0.75 GPa for high-density polyethylene) and complaint electrodes are used, the actuation strains can be significant and can result in fiber actuators that extend in length when an electric field is applied. Several examples of coaxial actuation have been demonstrated [4,5] but because of the fabrication methods the fibers have been short and have all had a hollow inner electrode. A consequence of the inner core being hollow rather than solid is that the tube can undergo an electro-mechanical instability in which the dielectric abruptly thins above a critical electric field. This was analyzed by Zhu et al. [5] for the conditions of a thin-walled tube configuration, namely, the dielectric is much thinner than the diameter of the tube.

Solid inner core coaxial elastomer fibers can now be fabricated in arbitrary lengths by 3D printing in which the dielectric and conductive electrode materials are co-extruded through a compound nozzle [6]. By varying the nozzle dimensions, the radii of the core, the dielectric annulus, and the outer electrodes can all be systematically varied. The electrode materials consist of an elastomer loaded with hydrophobic carbon black particles above the electrical percolation threshold concentration such that the electrodes are both elastically compliant and electrical conducting. The solid core ensures that the fibers do not undergo the electro-mechanical "thinning" instability. As the fibers can be printed, not only long fibers can be produced but also they can be formed in bundles as well as into complex curved shapes, such as cylinders [6]. In these geometries, the fibers are subject to bending.

In this work, the electro-mechanical stability of solid core coaxial elastomer fibers is considered. The critical instabilities are bifurcation modes associated with non-axisymmetric perturbations in electro-static charge distribution and the associated deformations and tractions of the fiber interfaces. The paper begins in Sec. 2 with an analysis of the stresses and deformation of a perfectly concentric three-component coaxial fiber comprised of neo-Hookean materials. The non-axisymmetric stability analysis is carried out in Sec. 3 with some of the analytic details given in the Supplemental Material on the ASME Digital Collection. The stability analysis requires a tightly coupled approach. The non-axisymmetric deformations produce non-axisymmetric changes in the electro-static charge distribution and in the associated electro-static tractions acting on the fiber interfaces, and vice versa. The limit of the three-component fiber wherein the modulus of the outer elastomeric annular sheath is set to zero and the outer surface remains conducting corresponds to a well-defined two-component system which is analyzed and discussed in Sec. 4. The two-component fiber with a rigid core, in turn, leads to consideration of a basic limiting problem: a planar elastomeric layer with conducting surfaces with one surface bonded to a rigid substrate and the other traction-free. This problem, which is solved in Ref. [7] and summarized in Sec. 5, provides additional fundamental insights into the nature of the electro-mechanical instability.

## 2 The Stresses and Deformation of the Perfectly Concentric Three-Component Fiber

The undeformed geometry of the three-component coaxial fiber is defined by an inner conducting core of radius $a_0$, surrounded by and bonded to a concentric non-conducting dielectric annulus with outer radius $b_0$, which, in turn, is bonded to a conducting annular sheath with outer radius $c_0$, as depicted in Fig. 1. The length of the fiber in the undeformed state is $L_0$ which is assumed to be much greater than $c_0$. The core (denoted by $A$) and the annular regions (denoted by $B$ and $C$, respectively) are made of incompressible, isotropic neo-Hookean elastomeric materials with ground state shear moduli $\mu_A$, $\mu_B$, and $\mu_C$. The interface at $r_0 = a_0$ is identified by the label $AB$ and that at $r_0 = b_0$ by $BC$. These interfaces do not resist deformation in any way other than through their

Contributed by the Applied Mechanics Division of ASME for publication in the Journal of Applied Mechanics. Manuscript received February 12, 2021; final manuscript received February 19, 2021; published online March 26, 2021. Assoc. Editor: Yonggang Huang.

  

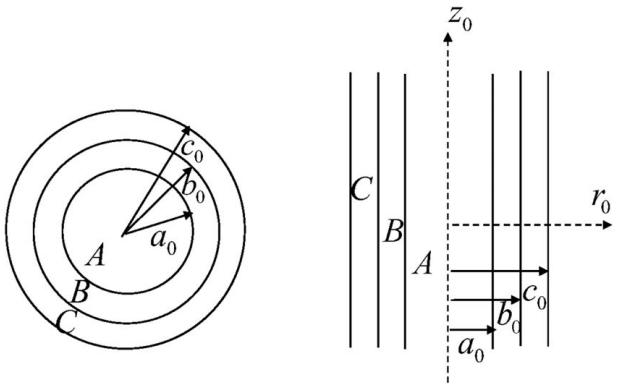


**Fig. 1 The three-component system in the undeformed state. The shear moduli in the respective components are $\mu_A$, $\mu_B$, and $\mu_C$. The interface between *A* and *B* is denoted by *AB* and that between *B* and *C* by *BC*.**

electro-static interaction driven by an imposed voltage difference across them.

The electro-static forces conspire to elongate the fiber in the $z$-direction. Away from the ends of the fiber (end details will not concern us here), the axial stretch $\lambda_z$ will be the same in each component. A basic consequence of incompressibility and cylindrical symmetry (and the absence of a cylindrical hole at the center of the fiber) is that any material point at radius $r_0$ in the undeformed body will be at radius $r = r_0/\sqrt{\lambda_z}$ in the deformed body. In particular, the radii of the two interfaces and the outer surface in the deformed state are $a = a_0/\sqrt{\lambda_z}$, $b = b_0/\sqrt{\lambda_z}$, and $c = c_0/\sqrt{\lambda_z}$, and the deformed length is $L = \lambda_z L_0$. Note also that $a/b = a_0/b_0$ and $c/b = c_0/b_0$. Furthermore, since the circumferential stretch of a material element at initial radius $r_0$ is $\lambda_\theta = r/r_0$, it follows that $\lambda_\theta = 1/\sqrt{\lambda_z}$. Incompressibility ($\lambda_r\lambda_\theta\lambda_z = 1$) gives $\lambda_r = 1/\sqrt{\lambda_z}$. In summary, incompressibility and cylindrical symmetry and otherwise independent of any constitutive assumptions, the stretches are uniform throughout the fiber and are given by

$$\lambda_r = \lambda_\theta = 1/\sqrt{\lambda_z} \tag{2.1}$$

with $\lambda_z$ to be determined.

The electrical charge associated with the imposed voltage $V_0$ resides on the two interfaces, $AB$ and $BC$, of the conducting components. A direct calculation of the radial tractions given in the Supplemental Material on the ASME Digital Collection provides the tractions (force per area) acting on the two interfaces due to the electro-static forces

$$\mathbf{T}^{AB} = \frac{\varepsilon V_0^2}{2(a\ln(b/a))^2}\mathbf{i}_r \equiv T^{AB}\mathbf{i}_r \quad \text{and}$$
$$\mathbf{T}^{BC} = -\frac{\varepsilon V_0^2}{2(b\ln(b/a))^2}\mathbf{i}_r \equiv T^{BC}\mathbf{i}_r \tag{2.2}$$

with $\varepsilon$ as the permittivity of the dielectric material in $B$, $a$ and $b$ as the radii in the deformed state of the perfectly concentric fiber, and $\mathbf{i}_r$ as the unit vector pointing in the radial direction. The electrical energy stored in the perfectly concentric fiber is

$$\Psi_{\text{electric}} = \frac{\pi\varepsilon L V_0^2}{\ln(b/a)} \equiv \frac{1}{2}CV_0^2 \tag{2.3}$$

where $C$ is the fiber capacitance in the current state.

The neo-Hookean strain energy density function is given by

$$W = \frac{1}{2}\mu(\lambda_r^2 + \lambda_\theta^2 + \lambda_z^2 - 3) \tag{2.4}$$

where $(\lambda_r, \lambda_\theta, \lambda_z)$ are the principal stretches which are aligned with the cylindrical coordinates $(r, \theta, z)$ in the pre-bifurcation state and the modulus is denoted by $\mu_A$, $\mu_B$, or $\mu_C$ in the respective components. The incompressibility condition, $\lambda_r\lambda_\theta\lambda_z = 1$, must be imposed. The true stresses are related to the stretches by

$$\sigma_r = \mu\lambda_r^2 - q, \quad \sigma_\theta = \mu\lambda_\theta^2 - q, \quad \sigma_z = \mu\lambda_z^2 - q \tag{2.5}$$

where $q$ is related to the pressure and is determined by equilibrium considerations. The stresses will be seen to be uniform in each component.

Under prescribed voltage $V_0$, the free energy of the coaxial fiber system is the sum of the elastic energy and the potential energy of the battery maintaining the voltage:

$$\Psi(\lambda_r, \lambda_\theta, \lambda_z, V_0) = \Psi_{\text{elastic}} - \Psi_{\text{electric}} \quad \text{and}$$
$$\Psi_{\text{elastic}} = 2\pi L_0\int_0^{c_0} W(\lambda_r, \lambda_\theta, \lambda_z)\, r_0 dr_0 \tag{2.6}$$

This is a mixed formulation in that the elasticity is Lagrangian employing the undeformed state as reference, while the electrical potential energy is defined in the current, deformed state. With $u_r(r_0)$ as the radial displacement, $\lambda_r = 1 + du_r/dr_0$ and $\lambda_\theta = 1 + r_0^{-1}u_r$. Rendering the free energy stationary for fixed voltage with respect to all admissible variations $\delta u_r$ and $\delta\lambda_z$ requires

$$2\pi L_0\int_0^{c_0}(-\sigma_r\lambda_\theta\lambda_z + \sigma_\theta\lambda_r\lambda_z)\delta u_r dr_0 + 2\pi L_0\int_0^{c_0}\sigma_z\lambda_z^{-1}\delta\lambda_z r_0 dr_0$$
$$+ 2\pi a_0 L_0\lambda_\theta\lambda_z(\sigma_r^A - \sigma_r^B)\delta u_r(a_0)$$
$$+ 2\pi b_0 L_0\lambda_\theta\lambda_z(\sigma_r^B - \sigma_r^C)\delta u_r(b_0)$$
$$+ \frac{\pi\varepsilon V_0^2 L}{[\ln(b/a)]^2}\left(\frac{\delta u_r(b_0)}{b} - \frac{\delta u_r(a_0)}{a}\right) - \frac{\pi\varepsilon V_0^2 L_0}{\ln(b/a)}\delta\lambda_z = 0 \tag{2.7}$$

Above, use has been made of the fact that $\partial W/\partial\lambda_i = N_i$ are the nominal stresses (force/original area) which are related to the true stresses (force/current area) by $N_r = \sigma_r\lambda_\theta\lambda_z$, $N_\theta = \sigma_\theta\lambda_r\lambda_z$, and $N_z = \sigma_z\lambda_r\lambda_\theta$. The integration by parts employed in arriving at (2.7) anticipates; $\sigma_r$ is uniform within each component; $\sigma_r^A$ denotes the radial stress within component $A$, etc.

Noting that $\lambda_\theta\lambda_z = \lambda_r\lambda_z = \lambda_z^{1/2}$ throughout the fiber, the first integral in (2.7) requires $\sigma_\theta = \sigma_r$ which could have been anticipated. Enforcing (2.7) for all variations $\delta u_r(a_0)$ and $\delta u_r(b_0)$ requires

$$(\sigma_r^A - \sigma_r^B) = \frac{\varepsilon V_0^2}{2a^2[\ln(b/a)]^2} = T^{AB} \quad \text{and}$$
$$(\sigma_r^B - \sigma_r^C) = -\frac{\varepsilon V_0^2}{2b^2[\ln(b/a)]^2} = T^{BC} \tag{2.8}$$

These equations balance the electro-static normal interface tractions, $T^{AB}$ and $T^{BC}$, introduced earlier in (2.2), by the stresses in the components. These conditions emerge naturally in rendering the free energy of the system stationary. Stationarity with respect to $\delta\lambda_z$ requires

$$2\pi\int_0^{c_0}\sigma_z\lambda_z^{-1} r_0\, dr_0 = \frac{\pi\varepsilon V_0^2}{\ln(b/a)} \tag{2.9}$$

which becomes the equation for determining the axial stretch in terms of the stresses

$$(a_0^2\sigma_z^A + (b_0^2 - a_0^2)\sigma_z^B + (c_0^2 - b_0^2)\sigma_z^C)\lambda_z^{-1} = \frac{\varepsilon V_0^2}{\ln(b/a)} \tag{2.10}$$

The final step in the calculation is to solve for the stresses using the constitutive relations (2.5) together with (2.8). The outer surface of the fiber is traction-free: $\sigma_r^C = \mu_C\lambda_z^{-1} - q_C = 0$. It then immediately follows that

$$\sigma_\theta^C = \mu_C\lambda_z^{-1} - \mu_C\lambda_z^{-1} = 0 \quad \text{and} \quad \sigma_Z^C = \mu_C(\lambda_z^2 - \lambda_z^{-1}) \tag{2.11}$$

At $r=b$, the second balance equation in (1.8) must be satisfied, requiring $\sigma_r^B = T^B$ such that $\mu_B \lambda_z^{-1} - q_B = T^B$. Thus,

$$\sigma_r^B = \sigma_\theta^B = T^{BC} \quad \text{and} \quad \sigma_z^B = \mu_B(\lambda_z^2 - \lambda_z^{-1}) + T^{BC} \tag{2.12}$$

At $r=a$, the radial stresses in $A$ and $B$ must balance $T^{AB}$ (first equation in (2.8)) requiring $\sigma_r^A - \sigma_r^B = T^{AB}$ with the following results for the components of stress in $A$

$$\begin{aligned} &\sigma_r^A = \sigma_\theta^A = T^{AB} + T^{BC} \quad \text{and} \\ &\sigma_z^A = \mu_A(\lambda_z^2 - \lambda_z^{-1}) + T^{AB} + T^{BC} \end{aligned} \tag{2.13}$$

Finally, the equation for the axial stretch $\lambda_z$ is obtained by enforcing (2.10)

$$\lambda_z - \lambda_z^{-2} = \frac{\varepsilon V_0^2}{\ln(b_0/a_0)}(a_0^2\mu_A + (b_0^2 - a_0^2)\mu_B + (c_0^2 - b_0^2)\mu_C)^{-1} \tag{2.14}$$

remembering that $b/a = b_0/a_0$ and using the fact that $a_0^2(T^{AB} + T^{BC}) + (b_0^2 - a_0^2)T^{BC} = 0$, in agreement with the result in Ref. [6]. In dimensionless form, this equation can be written as

$$\lambda_z - \lambda_z^{-2} = \frac{\Omega_0}{\ln(b_0/a_0)}\left(\left(\frac{a_0}{b_0}\right)^2\frac{\mu_A}{\mu_B} + \left(1 - \left(\frac{a_0}{b_0}\right)^2\right) + \left(\left(\frac{c_0}{b_0}\right)^2 - 1\right)\frac{\mu_C}{\mu_B}\right)^{-1} \tag{2.15}$$

with

$$\Omega_0 = \frac{\varepsilon V_0^2}{\mu_B b_0^2} \quad \text{or} \quad \sqrt{\Omega_0} = \sqrt{\frac{\varepsilon}{\mu_B}}\frac{|V_0|}{b_0}$$

The plots in Fig. 2 set the stage by illustrating theoretical and experimental trends in the axial strain, $\varepsilon_z = \lambda_z - 1$, as dependent on voltage and the radius ratio $a_0/b_0$. Figure 2(*a*) presents the strain as a function of the dimensionless voltage load parameter $\sqrt{\Omega_0}$ from (2.15) for six radius ratios with outer sheath radius set at $b_0/c_0 = 0.95$ and with $\mu_A = \mu_B = \mu_C \equiv \mu$. For the cylindrical geometry of the three-component fiber, the axial stretch increases monotonically with increases in the voltage parameter. For large $|V_0|$, by (2.15), $\lambda_z$ increases linearly with $V_0^2$. One implication of this result is that an axisymmetric instability mode akin to necking is unlikely to exist for solid core coaxial fibers made from neo-Hookean materials or from other elastomeric materials that display stiffening under stretch. The first occurrence of instability of the perfect fibers in Fig. 2(*a*) is indicated by the solid black dot obtained from the analysis in Sec. 3. The instability is a non-axisymmetric bifurcation with circumferential mode number $m$. Figure 2(*b*) presents a comparison of experimental data for axial strain (in percent) as a function of voltage from Ref. [6] for three fibers with predictions from (2.15), including the onset of the lowest non-axisymmetric bifurcation from the analysis of Sec. 3. The termination of the experimental curves in Fig. 2(*b*) is associated with electrical breakdown. The properties of the fibers (taken from [6]) are $\mu_A = \mu_C = 114$ kPa, $\mu_B = 155$ kPa, and $\varepsilon = 24.8 \times 10^{-12}$ NV$^{-2}$, with the component radii ($a_0$, $b_0$, $c_0$) of the three fibers in $\mu m$ as (205, 361, 372), (110, 332, 347), and (53, 339, 356).

The onset of the instability in the form of the non-axisymmetric bifurcation will be analyzed and discussed in the next section, but several observations to set the stage can be made based on the results in Fig. 2. First, the onset of instability has a strong geometric dependency. Figure 2(*a*) already reveals that instability is significantly postponed for fibers in the range $0.3 < a_0/b_0 < 0.5$. Second, none of the fibers in Ref. [6] in Fig. 2(*b*) reached the onset of instability. Nevertheless, a systematic increase in the axial strain above the theoretical prediction for the axisymmetric fiber occurs when the voltage exceeds about 50% of the instability onset predicted for the perfect fiber. One possible explanation for this behavior is that it is driven by non-axisymmetric imperfections—such behavior is common in structural buckling problems at loads on the order of 50% of the buckling load. It is also worth noting that, in the range of strains associated with the results in Fig. 2, the neo-Hookean material model should be a good representation of isotropic elastomeric materials.

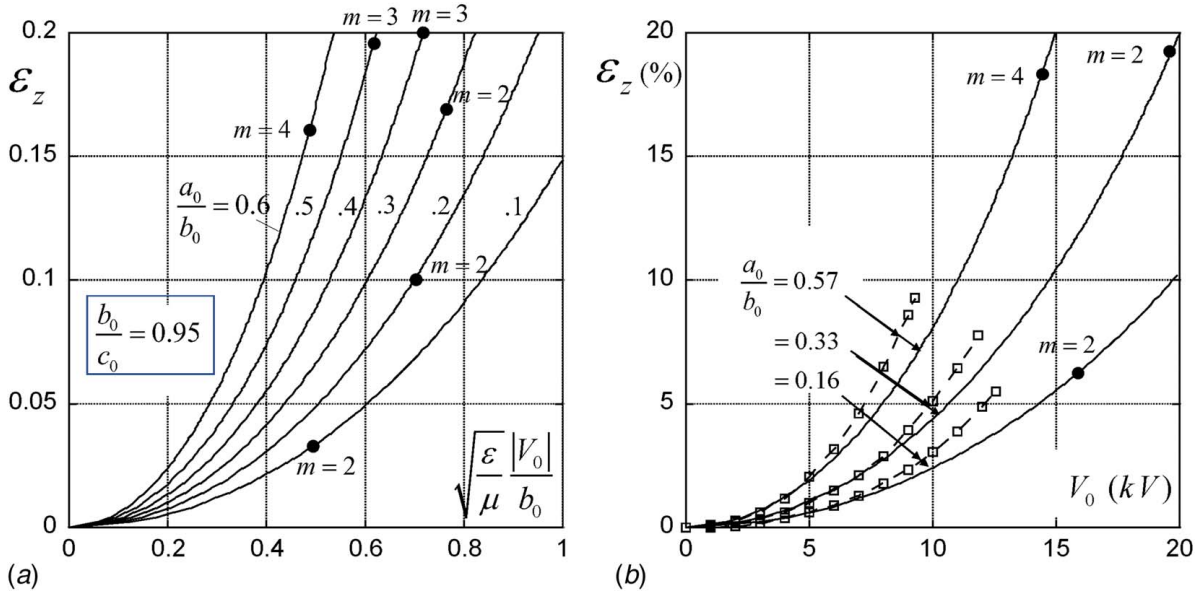


**Fig. 2 (*a*) Dependence of axial strain on the dimensionless voltage parameter for six three-component fibers over a range of the radii ratio $a_0/b_0$ for components with identical shear moduli $\mu$ predicted by (2.15). (*b*) Experimentally measured actuation axial strain as dependent on applied voltage (square points and dashed curves) for three fibers tested in Ref. [6] with properties listed in the text. The solid curves are the predictions for these fibers from (2.15). In both (*a*) and (*b*), the black circular point on each of the theoretical curves marks the onset of instability of the axisymmetric state as determined in Sec. 3. The index $m$ is the circumferential mode number as detailed in Sec. 3. The termination of the experimental curves is due to electrical breakdown.**

## 3 Non-Axisymmetric Bifurcation From the Concentric State for the Three-Component Fiber

The perfectly concentric fiber loses stability as a non-axisymmetric bifurcation from the pre-bifurcation state detailed in Sec. 2. At the point of bifurcation, the geometry of the fiber is specified by $a = a_0/\sqrt{\lambda_z}$, $b = b_0/\sqrt{\lambda_z}$, $c = c_0/\sqrt{\lambda_z}$, and $L = L_0\lambda_z$. The cylindrical coordinate system $(r, \theta, z)$ in the pre-bifurcation state with $r = r_0/\sqrt{\lambda_z}$ and $z = z_0\lambda_z$ will be used in the bifurcation analysis such that in $A$, $0 \le r \le a$, etc. We will focus our attention on plane strain bifurcations, with $\lambda_z$ fixed at the value given by (2.15). The equations governing bifurcation admit modes with incremental changes in displacements and in $q$ from the pre-bifurcation state, $(\dot{u}_r, \dot{u}_\theta, \dot{u}_z, \dot{q})$, of the separable form

$$\dot{u}_r = U(r)\cos m\theta, \quad \dot{u}_\theta = V(r)\sin m\theta, \quad \dot{u}_z = 0, \qquad \dot{q} = Q(r)\cos m\theta, \quad m = 1, 2, 3, \ldots \tag{3.1}$$

with incompressibility requiring

$$U' + r^{-1}(U + mV) = 0 \tag{3.2}$$

where $(\,)' = d(\,)/dr$.

The full details of the electro-static problem in the bifurcated state are given in the Supplemental Material on the ASME Digital Collection. The analysis conducted in this paper requires the lowest order changes in the electro-static tractions and the work they perform on interfaces $AB$ and $BC$. These lowest order changes are determined by perturbing about the axisymmetric pre-bifurcation state using $U(a)/a$ and $U(b)/b$ as the amplitudes of the shape perturbations. The electro-static tractions on the two interfaces subject to fixed $V_0$ are

$$\mathbf{T}^{AB} = \frac{\varepsilon V_0^2}{2[a\ln(b/a)]^2}\left\{1 + \left(\frac{2((m-1)+(m+1)(a/b)^{2m})}{1-(a/b)^{2m}}\frac{U(a)}{a} - \frac{4m(a/b)^m}{1-(a/b)^{2m}}\frac{U(b)}{b}\right)\cos m\theta\right\}\mathbf{n}_{AB} \tag{3.3}$$

$$\mathbf{T}^{BC} = \frac{\varepsilon V_0^2}{2[b\ln(b/a)]^2}\left\{1 - \left(-\frac{4m(a/b)^m}{1-(a/b)^{2m}}\frac{U(a)}{a} + \frac{2((m+1)+(m-1)(a/b)^{2m})}{1-(a/b)^{2m}}\frac{U(b)}{b}\right)\cos m\theta\right\}\mathbf{n}_{BC} \tag{3.4}$$

where $\mathbf{n}_{AB}$ and $\mathbf{n}_{BC}$ are the unit normal to the respective interfaces pointing into component $B$. The work per current unit length performed by these tractions on the fiber through the shape perturbations is

$$\Delta\Psi_{\text{electric}} = \frac{\pi}{2}\frac{\varepsilon V_0^2}{[b\ln(b/a)]^2}\{H_{AA}U(a)^2 + H_{AB}U(a)U(b) + H_{BB}U(b)^2\} \tag{3.5}$$

with

$$H_{AA} = \frac{(m-1)(b/a)^2 + (m+1)(a/b)^{2(m-1)}}{1-(a/b)^{2m}}, \quad H_{AB} = -\frac{4(a/b)^{m-1}}{1-(a/b)^{2m}}$$

$$H_{BB} = \frac{(m+1)+(m-1)(a/b)^{2m}}{1-(a/b)^{2m}}$$

The expression (3.5) is positive definite for all $U(a)$ and $U(b)$ for $0 < a/b < 1$. In other words, for shape changes in the form of any of the modes in (3.1), the battery maintaining the voltage $V_0$ does positive work on the fiber to lowest order in the bifurcation amplitudes. The axisymmetric pre-bifurcation tractions do no work through the bifurcation displacements.

For the mode with $m = 1$, (3.5) reduces to

$$\Delta\Psi_{\text{electric}} = \frac{\pi\varepsilon V_0^2}{[b\ln(b/a)]^2}\frac{1}{1-(a/b)^2}(U(b) - U(a))^2 \tag{3.6}$$

The mode in (3.1) for $m = 1$ implies that to lowest order in the bifurcation amplitude, the interfaces and the outer surface remain circular and simply undergo lateral translations relative to one another, as depicted in Fig. 3, even though straining occurs within the three components. In particular, the two interfaces, $AB$ and $BC$, on which the charge resides translate relative to each other by $\delta = U(b) - U(a)$. The result (3.6) is corroborated by the exact result in the literature [8] for the electrical energy per unit length stored in an cylindrical capacitor loaded to a voltage $V_0$ and having a circular inner conducting surface of radius $a$ and circular outer conducting surface of radius $b$ whose centers are offset

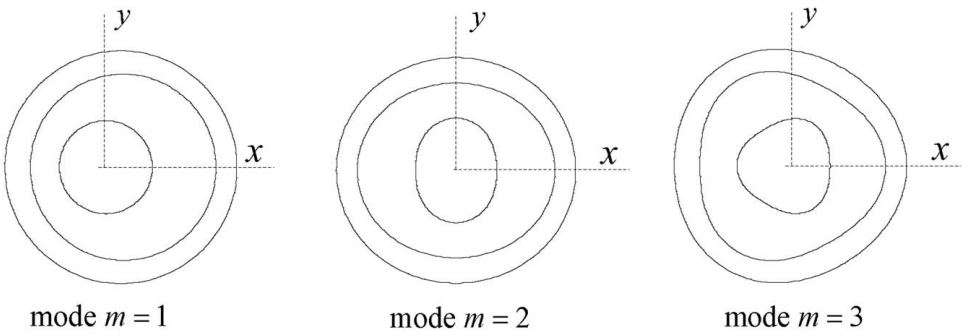


**Fig. 3 The plane strain bifurcation modes for $m = 1, 2, 3$**

from one another by a distance $\delta$:

$$\Psi_{\text{electric}} = \frac{\pi\varepsilon V_0^2}{\cosh^{-1}((a^2+b^2-\delta^2)/2ab)} = \frac{\pi\varepsilon V_0^2}{\ln(b/a)}\left\{1+\frac{\delta^2}{b^2\ln(b/a)(1-(a/b)^2)}+O(\delta^4)\right\} \tag{3.7}$$

The expression for lowest order change in the elastic energy per unit length due to bifurcation is also quadratic in $U$ and $V$; the result, derived in the Supplemental Material on the ASME Digital Collection, is

$$\Delta\tilde{\Psi}_{\text{elastic}} = \frac{\Delta\Psi_{\text{elastic}}}{\pi\mu_B b^2/2} = \int_0^{\tilde{c}} \tilde{M}\left\{\left(2\tilde{r}^{-2}(\tilde{U}+m\tilde{V})^2+\frac{1}{2}(\tilde{V}'-\tilde{r}^{-1}(m\tilde{U}+\tilde{V}))^2\right) + \bar{\sigma}(\tilde{V}'^2+\tilde{r}^{-2}(m\tilde{U}+\tilde{V})^2+2\tilde{r}^{-2}(\tilde{U}+m\tilde{V})^2)\right\}\tilde{r}d\tilde{r} \tag{3.8}$$

where the stress $\sigma \equiv \sigma_r = \sigma_\theta$ takes on the uniform pre-bifurcation value in each component as does the modulus $M = 2\mu(\lambda_z^2 + 2\lambda_z^{-1})/3 - 2(2\sigma^2+\sigma_z^2)/3$. The following dimensionless quantities have been employed: $(\tilde{U},\tilde{V}) = (U,V)/b$, $\tilde{r} = r/b$, $(\,)' = d(\,)/d\tilde{y}$, $\tilde{a} = a/b$, $\tilde{b} = 1$, and $\tilde{a} = a/b$. The dimensionless component-dependent stress and modulus are $\bar{\sigma} = \sigma/M$ and $\tilde{M} = M/\mu_B$; the incompressibility condition is $\tilde{U}' + \tilde{r}^{-1}(\tilde{U}+m\tilde{V}) = 0$.

The dimensionless work done by the perturbed electro-static tractions (3.5) is

$$\Delta\tilde{\Psi}_{\text{electric}} = \frac{\Delta\Psi_{\text{elastic}}}{\pi\mu_B b^2/2} = \frac{\Omega}{(\ln(b/a))^2}\{H_{aa}\tilde{U}(a)^2 + H_{ab}\tilde{U}(a)\tilde{U}(b) + H_{bb}\tilde{U}(b)^2\} \tag{3.9}$$

where

$$\Omega = \frac{\varepsilon V_0^2}{\mu_B b^2} = \Omega_0\lambda_z \tag{3.10}$$

The functional governing the bifurcation eigenvalue problem is

$$\Delta\tilde{\Psi} = \Delta\tilde{\Psi}_{\text{elastic}} - \Delta\tilde{\Psi}_{\text{electric}} \tag{3.11}$$

This functional is homogeneous of degree 2 in the modal displacements. The eigenvalue is $\Omega$ while $\bar{\sigma}$ and $\tilde{M}$ can be expressed in terms of $\Omega$, $\lambda_z$, and the shear modulus ratios. For any given $m$, $\Delta\tilde{\Psi} > 0$ at voltages below the lowest critical eigenvalue for all non-zero admissible functions $\tilde{U}$ and $\tilde{V}$. The critical eigenvalue is the lowest voltage for which $\Delta\tilde{\Psi} = 0$ for some non-zero combination of $\tilde{U}$ and $\tilde{V}$, and this combination is the eigenmode when appropriately normalized.

**3.1 Solution Procedure.** In each component, the field equations for the modal quantities in (3.1) generated by rendering the functional (3.11) stationary admit four linearly independent solutions (see Supplemental Material on the ASME Digital Collection). For $m = 1$, the general solution in each component has the form

$$\tilde{U} = b_1 + b_2\tilde{r}^2 + b_3\tilde{r}^{-2} + b_4\ln\tilde{r},$$
$$\tilde{V} = -b_1 - 3b_2\tilde{r}^2 + b_3\tilde{r}^{-2} - b_4(\ln\tilde{r}+1) \tag{3.12}$$
$$\bar{Q} = 4(1+2\bar{\sigma})\,b_2\tilde{r} + (1+2\bar{\sigma})\,b_4\tilde{r}^{-1}$$

where the $b$'s are undetermined coefficients and $\bar{Q} = Q/M$. For $m \geq 2$, the four independent solutions are

$$\tilde{U} = b_1\tilde{r}^{n_1} + b_2\tilde{r}^{n_2} + b_3\tilde{r}^{n_3} + b_4\tilde{r}^{n_4},$$
$$\tilde{V} = b_1v_1\tilde{r}^{n_1} + b_2v_2\tilde{r}^{n_2} + b_3v_3\tilde{r}^{n_3} + b_4v_4\tilde{r}^{n_4} \tag{3.13}$$
$$\bar{Q} = b_2q_2\tilde{r}^{n_2-1} + b_3q_3\tilde{r}^{n_3-1}$$

where $n_1 = m-1$, $n_2 = m+1$, $n_3 = -(m-1)$, $n_4 = -(m+1)$, $v_i = -(n_i+1)/m$, $i = 1, 4$, $q_2 = 2(m+1)(1+2\bar{\sigma})/m$, and $q_3 = 2(m-1)(1+2\bar{\sigma})/m$. Each contribution in (3.12) and (3.13) satisfies the incompressibility condition. Denote the coefficients in component $A$ by $a_i$, $i = 1, 4$, in $B$ by $b_i$, $i = 1, 4$, and in $C$ by $c_i$, $i = 1, 4$.

It will now be shown that the bifurcation solution can be reduced to a form dependent only on the $b_i's$ in $B$ as independent unknowns. The solution must be bounded at the origin requiring $a_3 = a_4 = 0$. Continuity of $\tilde{U}$ and $\tilde{V}$ at $\tilde{r} = \tilde{a}$ provides two linear equations for $a_1$ and $a_2$ in terms of the $b_i's$. Four linear equations for $c_i$, $i = 1, 4$ in terms of the $b_i's$ are obtained from the two traction-free conditions at $\tilde{r} = \tilde{c}$ and the two continuity conditions on $\tilde{U}$ and $\tilde{V}$ at $\tilde{r} = \tilde{b}$. Thus, $a_1$, $a_2$ and $c_i$, $i = 1, 4$ are uniquely determined for every set of $b_i's$. For $m \geq 2$, $b_i$, $i = 1, 4$, are the free variables in solving the bifurcation problem. For $m = 1$, the set of free variables must be restricted to exclude the rigid body translation (i.e., $\tilde{U} = -\tilde{V} = \text{constant}$). This is achieved by taking $a_1 = 0$ such that the two interface continuity equations at $\tilde{r} = \tilde{a}$ provide equations for $a_2$ and one of the $b_i's$, which we have taken to be $b_4$. Thus for $m = 1$, there are three independent free variables, $b_1$, $b_2$, and $b_3$. For $m = 1$, the reduction gives

$$a_2 = \frac{\ln\tilde{a}(-2b_2\tilde{a}^2+2b_3\tilde{a}^{-2})+b_1+b_2\tilde{a}^2+b_3\tilde{a}^{-2}}{\tilde{a}^2(1-2\ln\tilde{a})}, \qquad b_4 = \frac{2b_1+4b_3\tilde{a}^{-2}}{1-2\ln\tilde{a}} \tag{3.14}$$

$$c_1 = \frac{2(1+\tilde{c}^4)b_1+4\tilde{c}^4b_2+4b_3-(1-\tilde{c}^4)b_4}{2(1+\tilde{c}^4)}, \qquad c_2 = \frac{2b_2-2b_3+b_4}{2(1+\tilde{c}^4)}, \quad c_3 = -\tilde{c}^4c_2, \quad c_4 = 0 \tag{3.15}$$

The reduction for $m \geq 2$ is also straightforward but requires the use of a linear equation solver which does not need to be described here.

In summary, the bifurcation mode can be represented by some combination of $b_i's$ (absent $b_4$ as a free variable for $m = 1$). For any combination of the $b_i's$, the integrations in each component region in the bifurcation functional can be carried out either analytically, although this would be lengthy, or numerically to high precision. The bifurcation functional (3.11) has thus been reduced to a quadratic algebraic function of the $b_i's$ with $\Omega$ as the eigenvalue, i.e., $\Delta\tilde{\Psi}(\mathbf{b}, \Omega)$. Standard numerical methods are available for solving the critical (lowest) eigenvalue and the associated bifurcation mode for each $m$, as discussed in the Supplemental Material on the ASME Digital Collection.

**3.2 Critical Voltage for Three-Component Fibers.** Figure 4 presents the solution to the eigenvalue problem just described for circumferential wave numbers $m = 1, 5$ for the family of fibers considered in Fig. 2(*a*). For any geometry, the critical (lowest) eigenvalue which determines the onset of the instability of the perfect fiber is indicated by a solid black dot in Fig. 2. For this example, the critical circumferential mode number is $m = 2$ in the lowest range of $a_0/b_0$, switches to $m = 3$ in the intermediate range of $a_0/b_0$, and switches again to $m = 4$ for $a_0/b_0 > 0.52$. The critical voltage, $\sqrt{\varepsilon/\mu_B}|V_0|/b_0$, and the associated axial strain, $\varepsilon_z = \lambda_z - 1$,

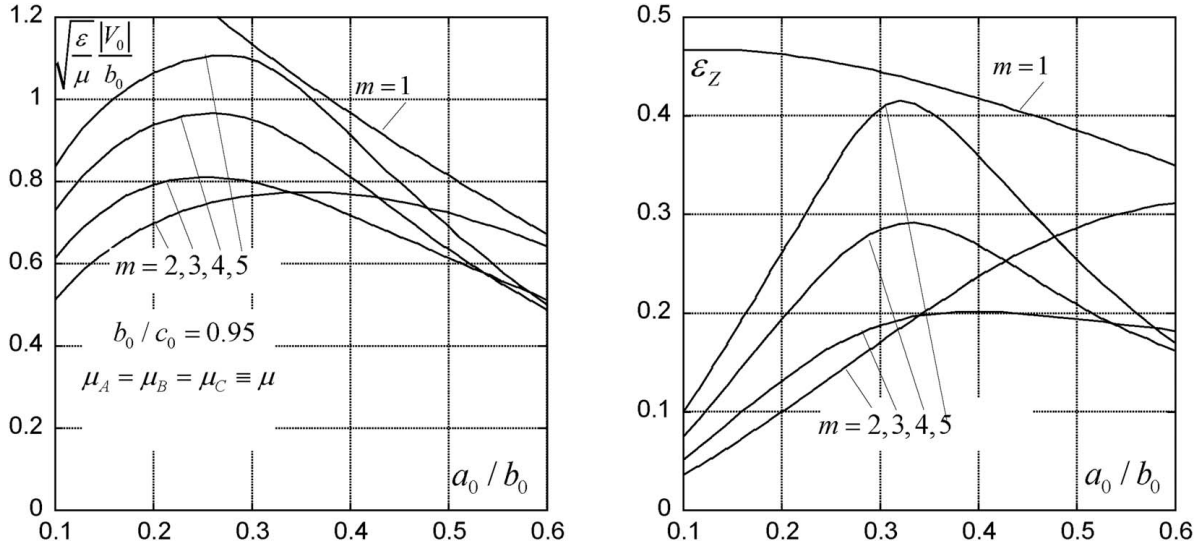


**Fig. 4 Instability eigenvalue spectrum $\sqrt{\Omega_0}=\sqrt{\varepsilon/\mu}|V_0|/b_0$ on the left and associated axial strain $\varepsilon_z$ on the right as dependent on $a_0/b_0$ and circumferential mode number $m$ for fibers with $b_0/c_0=0.95$ and identical component moduli $\mu$. The stability limits (black dots) in Fig. 2(a) are derived from these results.**

do not vary monotonically with $a_0/b_0$. The maximum critical voltage is attained for fibers having $a_0/b_0\cong 0.35$, but the maximum axial actuation strain at the onset of instability is $\varepsilon_z\cong 0.2$ throughout the range $0.35<a_0/b_0<0.52$.

Figure 5 reveals the influence of the shear modulus of the thin outer sheath for fibers with $a_0/b_0=0.5$ and $b_0/c_0=0.95$. Over the entire range of $\mu_C/\mu_B$ plotted, the critical voltage eigenvalue is associated with $m=3$. Relative to the case where the sheath and dielectric components have the same modulus, the critical voltage is reduced by about 20% when the sheath modulus becomes negligible compared to $\mu_B$ and it is increased by about 15% when $\mu_C=5\mu_B$. A sheath modulus with $\mu_C\cong\mu_B$ appears to be a good choice for maximizing the stable actuation strain range without unduly elevating the voltage for actuation. No formal optimization work will be conducted in this paper, but the stability analysis enables such studies.

In the examples discussed above, the mode with circumferential wave number $m=1$ is not competitive in the sense that the eigenvalue associated with this mode lies well above the critical mode having the lowest eigenvalue. This also will be the case for the two-component fibers discussed in the next section. Of all the plane strain circumferential modes considered in this paper, only the $m=1$ gives rise to a longitudinal bending moment (i.e., $M_x$ or $M_y$) in the fiber. The modes with $m\geq 2$ produce no longitudinal bending moment, and thus, an unconstrained, vertically supported fiber, as in the experiments in Ref. [6], would remain straight in the post-bifurcation range, at least for relatively small bifurcation displacements. If $m=1$ were critical, the fiber in such an experiment would undergo bending beyond the onset of instability. The moment for $m=1$ is computed in the Supplemental Material on the ASME Digital Collection, but it will not be discussed further here because this mode is not critical.

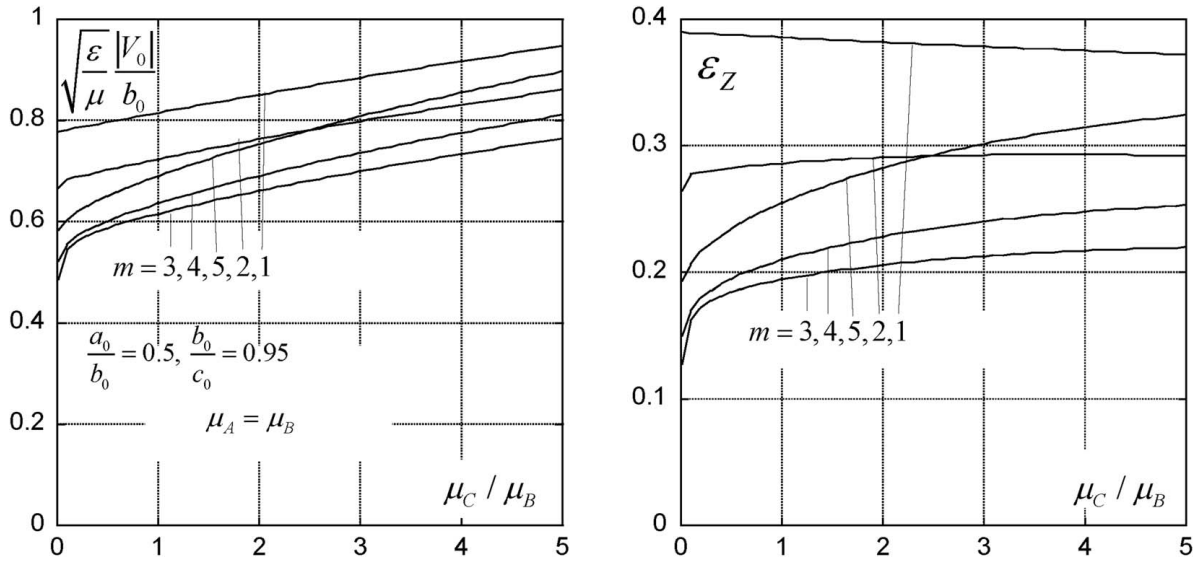


**Fig. 5 The influence of the sheath shear modulus on the voltage eigenvalue spectrum and the associated axial strain for fibers with $a_0/b_0=0.5$, $b_0/c_0=0.95$, and $\mu_A=\mu_B$**

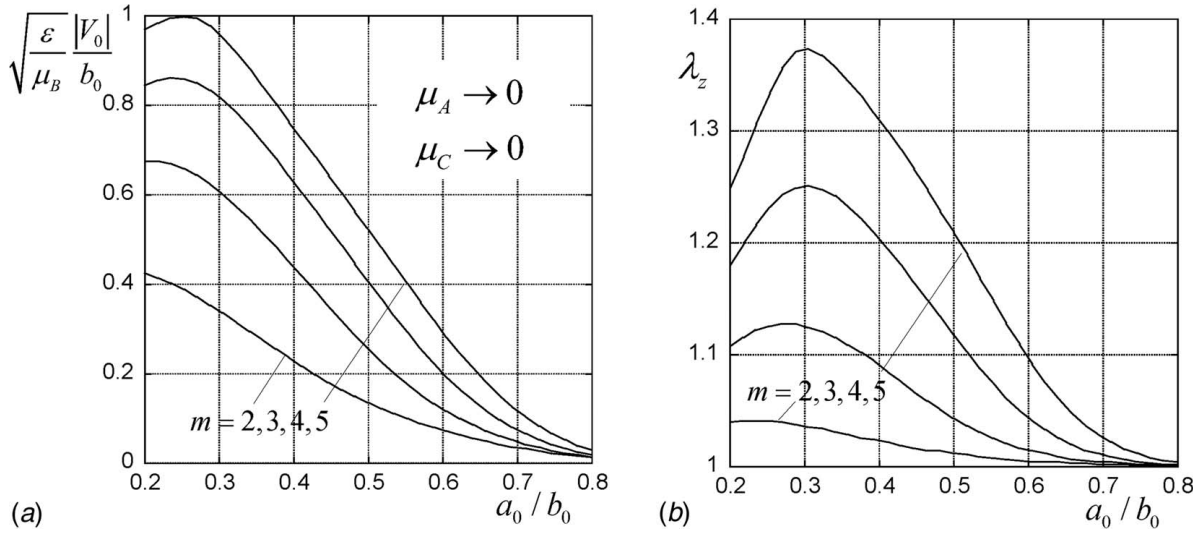


**Fig. 6 The dimensionless voltage eigenvalue spectrum in (*a*) and associated axial stretch in (*b*) for a two-component system with a fluid-filled core, *A*, and an elastomeric annulus, *B***

## 4 Critical Voltage for Two-Component Coaxial Fibers

If $\mu_C/\mu_B \to 0$, the solution method described in Sec. 3 generates solutions for the two-component system consisting of a conducting core $A$ and annulus $B$ with an outer conducting surface on $B$. Spectrums for the instability eigenvalue for the limiting cases of a fluid-filled core, $\mu_A/\mu_B \to 0$, and a rigid core, $\mu_A/\mu_B \to \infty$, are presented in Figs. 6 and 7. The associated axial stretch is shown for the fluid-filled core; the rigid core constrains the stretch to be unity.

The limit $\mu_C/\mu_B \to 0$ of the solution does not correspond to a core becoming a traction-free cavity [5], rather it corresponds to a conducting incompressible fluid with zero shear modulus which is assumed to be able to support the hydrostatic tension without cavitation in the core generated by the electro-static forces. In the limit of the fluid-filled core, the critical voltage is associated with the plane strain mode $m = 2$ over the entire range of geometry in Fig. 6. In this limit, it is possible that a plane strain mode is not the critical mode. Modes with both sinusoidal circumferential and axial variations should be considered including axisymmetric modes. The present analysis can be generalized to such modes [9], but lower instability possibilities for the fluid-filled core will not be pursued here.

The eigenvalue spectrum for rigid core fibers in Fig. 7 reveals that the circumferential wave number associated with the critical voltage eigenvalue depends strongly on $a_0/b_0$. The eigenvalue for $m = 2$ lies well above the critical eigenvalue over the entire range plotted, but the eigenvalue for $m = 1$ is the critical eigenvalue at the lower end of the interval, and it remains only modestly above the critical value over the entire interval. For values of $a_0/b_0$ at the upper range plotted, the critical eigenvalue approaches from above the asymptotic result derived in the next section:

$$\sqrt{\frac{\varepsilon}{\mu_B}}\frac{V_0}{b_0} = 1.2872\left(1 - \frac{a_0}{b_0}\right) \tag{4.1}$$

This asymptotic result becomes an increasingly accurate approximation as the ratio of the thickness of the annulus $B$ to $b_0$ becomes small. The result above holds in the limit of short wavelength modes that are increasingly confined to the vicinity of the outer free surface of component $B$, as will be discussed in the next section.

Figure 8 is a summary plot for the critical instability voltage and associated axial strain for two-component fibers showing results for five core-to-annulus shear modulus ratios.

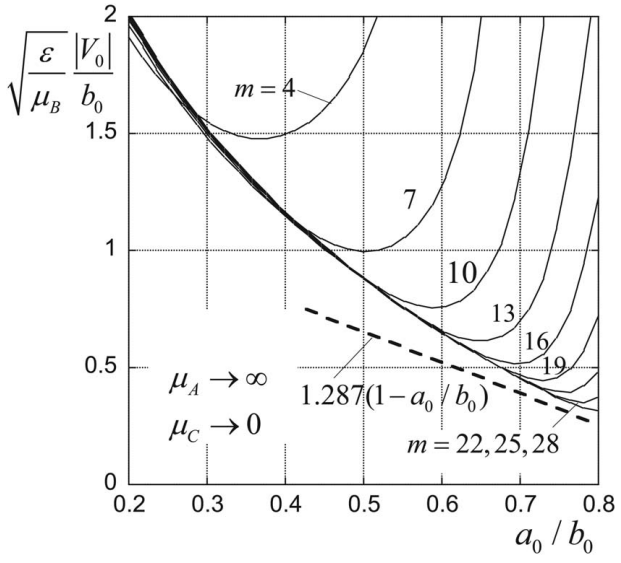


**Fig. 7 The dimensionless voltage eigenvalue spectrum for a two-component system with a rigid core, *A*, and an elastomeric annulus, *B*. The axial stretch is constrained by the core with $\lambda_z = 1$. Included as a dashed line is the asymptotic short wavelength limit in Sec. 5.**

## 5 A Dielectric Layer Clamped on the Bottom and Free at the Top

Motivated by the behavior noted in the previous section for the rigid core, consider as a special limiting case a planar incompressible neo-Hookean layer modeling the dielectric elastomer, of thickness $h$ and shear modulus $\mu$, that is bonded to a rigid substrate on the bottom and traction-free on the top. The upper and lower surfaces of the layer are conducting with a voltage $V_0$ imposed across them. This problem can be analyzed using the method laid out in Sec. 3. The bifurcation and initial post-bifurcation behavior of this problem and a companion problem have been analyzed in Ref. [7]. Experimental studies of versions of this planar problem have also been carried out [10,11]. Here we provide a summary of the results of the planar problem relevance to the two-component fiber with the rigid core.

Owing to the constraint of the rigid substrate, the pre-bifurcation state in the layer is one of hydrostatic compression:

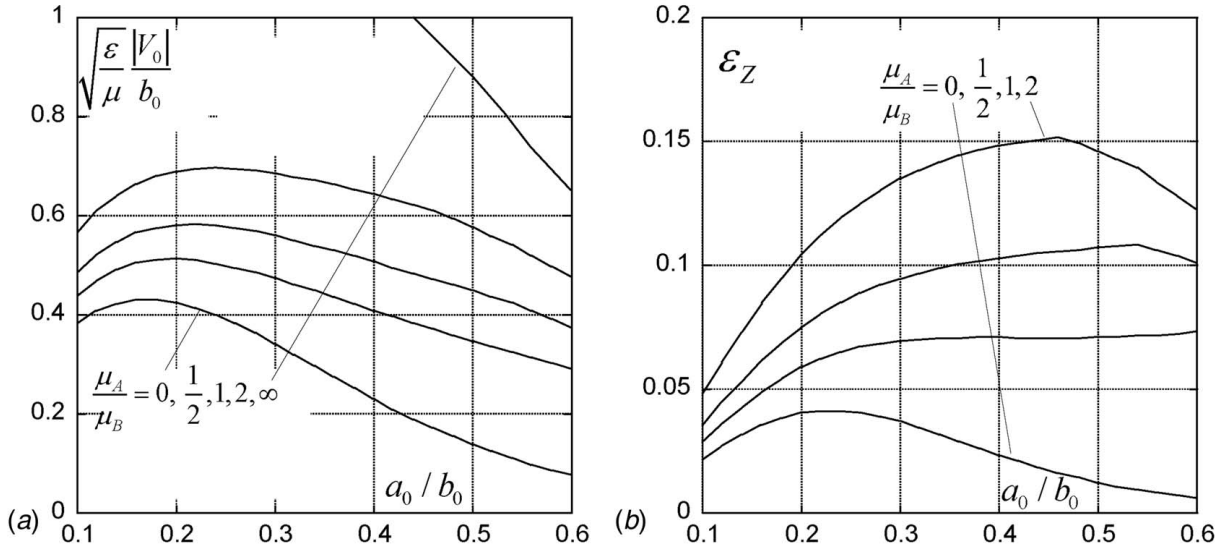


**Fig. 8 (*a*) Critical (lowest) voltage eigenvalue and (*b*) associated axial strain for two-component coaxial fibers for five ratios of core to annulus shear moduli ranging from fluid-filled cores to fibers with rigid cores. The axial strain for the rigid core fiber is zero.**

$\sigma_x = \sigma_y = \sigma_z = -\varepsilon V_0^2/2h^2$ with $\lambda_x = \lambda_y = \lambda_y = 1$ in the coordinates of the insert in Fig. 9. The pre-bifurcation thickness in the current state is unchanged from that in the unstressed state. Denote the plane strain displacement increments associated with the bifurcation solution by $\dot{u}_x = U(y)\sin(kx)$, $\dot{u}_y = V(y)\cos(kx)$, and $\dot{u}_z = 0$ with $k$ as the mode wave number and $\ell = 2\pi/k$ as the wavelength. On $y = 0$, $U = V = 0$. With a voltage $V_0$ prescribed across the top and bottom surfaces, the traction, $\mathbf{T}$, on the top perturbed surface and the lowest order work, $\Delta\Psi_{\text{electric}}$, done by these tractions per unit length in the $z$-direction over one wavelength $\ell$ are

$$\mathbf{T} = \frac{\varepsilon V_0^2}{2h^2}\left(1 - 2\frac{kh}{\tanh(kh)}\frac{V(h)}{h}\cos(kx)\right)\mathbf{n} \quad \text{and}$$
$$\Delta\Psi_{\text{electric}} = \frac{\pi\varepsilon V_0^2}{2h^2}\frac{1}{\tanh(kh)}V(h)^2 \tag{5.1}$$

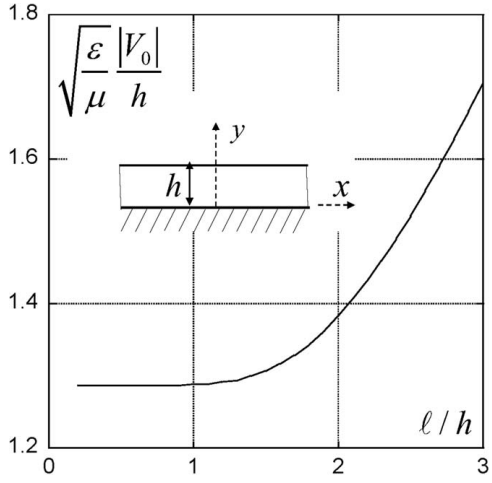


**Fig. 9 Spectrum of the voltage eigenvalue as a function of the wavelength for the infinite dielectric neo-Hookean layer. The top and bottom surfaces of the layer are conducting. The top surface is unconstrained and the bottom surface is bonded to a rigid substrate.**

with $\mathbf{n}$ as the unit normal to the top surface pointing into the layer. The dimensionless quadratic functional governing bifurcation is

$$\Delta\tilde{\Psi} = \int_0^1 \{(2+\Omega)(2(\tilde{k}\tilde{U})^2 + (\tilde{U}' - \tilde{k}\tilde{V})^2/2) - (\Omega/2)(\tilde{U}'^2 + 2(\tilde{k}\tilde{U})^2 + (\tilde{k}\tilde{V})^2)\}d\tilde{y} - \Omega(\tilde{k}/\tanh(\tilde{k}))\tilde{V}(1)^2 \tag{5.2}$$

with $\tilde{y} = y/h$, $(\,)' = d(\,)/d\tilde{y}$, $\tilde{k} = kh$, $(\tilde{U}, \tilde{V}) = (U, V)/h$, and $\Omega = \varepsilon V_0^2/(\mu h^2)$. The field equations admit linearly two linearly independent solutions after the boundary conditions on the bottom of the layer are satisfied:

$$\tilde{U} = -b_1\tilde{k}^2\tilde{y}\sinh(\tilde{k}\tilde{y}) + b_2(\sinh(\tilde{k}\tilde{y}) + \tilde{k}\tilde{y}\cosh(\tilde{k}\tilde{y}))$$
$$\tilde{V} = b_1(-\tilde{k}\sinh(\tilde{k}\tilde{y}) + \tilde{k}^2\tilde{y}\cosh(\tilde{k}\tilde{y})) - b_2\tilde{k}\tilde{y}\sinh(\tilde{k}\tilde{y}) \tag{5.3}$$

The eigenvalue spectrum as dependent on the dimensionless modal wavelength, $\ell/h = 2\pi/\tilde{k}$, is plotted in Fig. 9. An interesting feature of this spectrum is that for sufficiently short wavelengths, the eigenvalue becomes independent of the wavelength and given by

$$\sqrt{\Omega} = \sqrt{\frac{\varepsilon}{\mu}}\frac{|V_0|}{h} = 1.2872 \tag{5.4}$$

It can be seen from Fig. 9 that this limiting result is the critical eigenvalue governing planar stability of the layer and, moreover, the eigenvalue for a wavelength as large as $\ell/h = 1$ is less than 0.1% above (5.4). Although not evident from (5.3), the mode becomes increasingly concentrated at the top surface of the layer as the wavelength gets shorter and shorter.

The problem for the short wavelength limit in which the eigenvalue becomes independent of the wavelength is readily formulated. It corresponds to an infinitely deep layer with a conducting surface subject to an electric field in the vertical direction producing a gradient in the voltage potential of magnitude equal to $|V_0|/h$ ($h$ is no longer the layer thickness). In this formulation, with the vertical coordinate $y$ taken with its origin at the top surface, the short wavelength eigenmodes associated with the critical eigenvalue (5.4) turn

out to be

$$\dot{u}_x = \left(-1 + \sqrt{2}(1+ky)\right)e^{ky}\sin(kx) \quad \text{and}$$

$$\dot{u}_y = \left(1 - \sqrt{2}ky\right)e^{ky}\cos(kx)$$

In this form, it is evident that the bifurcation mode decays exponentially into the layer scaled by the wavelength $\ell = 2\pi/k$. This surface instability has much in common with the instability of a compressed neo-Hookean half-space with a traction-free surface first analyzed by Biot [12], although in the present problem the pre-bifurcation state is hydrostatic compression with no strain. Because the arbitrarily short wavelength modes are localized near the surface, the result in (5.4) implies that surface instabilities will occur at any location on a conducting traction-free surface when the magnitude of the electric field gradient normal to the surface exceeds the limit associated with (5.4), assuming the elastomer is constrained below the surface.

To address the relevance of (5.4) to the two-component coaxial fiber with the rigid core, consider geometries such that the distance between the conducting surfaces of the fiber, $h = b_0 - a_0$, the inner one fully constrained and the other unconstrained, is relatively small compared to $b_0$. If $h$ is replaced by $b_0 - a_0$ in (5.4), one obtains

$$\sqrt{\frac{\varepsilon}{\mu_B}}\frac{|V_0|}{b_0} = 1.2872\left(1 - \frac{a_0}{b_0}\right) \tag{5.5}$$

with the modulus identified as that of $B$. This is the result plotted as a dashed line in Fig. 7.

The post-bifurcation analysis of the constrained layer in Ref. [7] sheds light on the nature of the instability at bifurcation. The short wavelength modes are highly unstable, and the maximum attainable voltage is reduced below the bifurcation value by small imperfections in the system. In the physics community, such instabilities are referred to as subcritical implying a bifurcated solution is associated with falling voltage. Experiments on constrained planar layers [10,11] reveal that the instability occurs as a dynamic snaping from the nominally planar state to localized crease-like entities. Therefore, it is logical to conclude that the short wavelength modes on the fibers with rigid cores will similarly be highly unstable and imperfection sensitive. Post-bifurcation analyses have not been performed for the coaxial fiber modes with small circumferential wavenumbers, i.e., $m = 1, 2, 3, \ldots$, nor have experimental observations been reported which would indicate whether the bifurcation is subcritical or supercritical.

## 6 Conclusions

Current coaxial elastomer fibers are produced by co-extrusion of the core, dielectric, and outer electrode so there exists the possibility of local variations in the radii of these components as well as non-perfect axial symmetry of the fibers. No direct evidence for the formation of any voltage-induced bifurcations has been observed, although as discussed below the electrical breakdown which terminates the actuation strains in Ref. [6] may be triggered by the instability. Neither has any crease-like post-bifurcation associated with short wavelength surface modes yet been observed for the fibers. However, the analysis presented in this work suggests that they may exist, although at electric fields not hitherto reached because electrical breakdown provoked by other effects has intervened. Of particular interest, since complex shapes can be produced by 3D printing, is the possible occurrence of instabilities in lengths of fibers bent prior to the application of a voltage. In a bent coaxial fiber, there will be azimuthal variations in the thickness of the dielectric and consequently non-axisymmetric electric fields.

The behavior of the coaxial fibers tested in Ref. [6] compared with the theoretical predictions for their perfect counterparts in Fig. 2(*b*) reveals that noticeably larger axial strains than those predicted begin to appear at voltages which are roughly one half of the voltage predicted for the onset of instability. It is possible that the larger strains might be due to the manufacturing imperfections referred to above, particularly if the critical bifurcation turns out to be subcritical, which has yet to be established except for the short wavelength modes. If bifurcation for the modes with $m = 1, 2, 3, \ldots$ is also subcritical, then it is possible, and perhaps even likely, that the maximum voltages achieved in the experiments in Ref. [6] could be due to the instabilities investigated in this paper. In the experiments, the maximum voltage attained is associated by electrical breakdown occurring in the range between 50% and 80% of the bifurcation prediction (cf., Fig. 2(*b*)). Imperfections in the fiber could be responsible for prematurely triggering the instability which in turn would bring about the electrical breakdown.


## Acknowledgment

JWH is indebted to A. David Wunch for discussion on issues related to the electro-statics and for calling his attention to Ref. [8]. This research was supported by NSF through the Harvard University Materials Research Science and Engineering Center DMR-2011754.


## Conflict of Interest

There are no conflicts of interest.

## Data Availability Statement

The datasets generated and supporting the findings of this article are obtained from the corresponding author upon reasonable request. The authors attest that all data for this study are included in the paper.

## References


[1] Pelrine, R., Kornbluh, R., Pei, Q., and Joseph, J., 2000, "High-Speed Electrically Actuated Elastomers With Strain Greater Than 100," Science, **287**(5454), pp. 836–839.

[2] Suo, Z., 2010, "Theory of Dielectric Elastomers," Acta Mech. Sol. Sin., **28**(6), pp. 549–578.

[3] Zhao, H., Hussain, A. M., Dudula, M., Vogt, D. M., Wood, R., and Clarke, D. R., 2018, "Compact Dielectric Elastomer Linear Actuators," Adv. Funct. Mater., **28**(42), p. 1804828.

[4] Carpi, F., and De Rossi, D., 2004, "Dielectric Elastomer Cylindrical Actuators: Electromechanical Modelling and Experimental Evaluation," Mater. Sci. Eng. C, **24**(4), pp. 555–562.

[5] Zhu, J., Stoyanov, H., Kofod, G., and Suo, Z., 2010, "Large Deformation and Electromechanical Instability of a Dielectric Elastomer Tube Actuator," J. Appl. Phys., **108**(7), p. 074113.

[6] Chortos, A., Mao, J., Mueller, J., Hajiesmaili, E., Lewis, J. A., and Clarke, D. R., in press, "Printing Reconfigurable Bundles of Dielectric Elastomer Fibers," Adv. Funct. Mater.

[7] Hutchinson, J. W., in press, "Surface Instabilities of Constrained Elastomeric Layers Subject to Electro-Static Stressing."

[8] Bewley, L. V., 1948, *Two Dimensional Fields in Electrical Engineering*, Macmillan, New York.

[9] Hutchinson, J. W., 2020, "Instabilities of Embedded Cylindrical Inclusions Undergoing Isotropic Swelling or Growth," Extreme Mech. Lett., **40**, pp. 1–6.

[10] Kofod, G., Kornbluh, R., Pelrine, R., and Sommer-Larson, P., 2003, "Actuation Response of Polyacrylate Dielectric Elastomers," J. Intell. Mater. Syst. Struct., **14**(12).

[11] Wang, Q., Tahir, M., Zhang, L., and Zhao, X., 2011, "Electro-Creasing Instability in Deformed Polymer Experiments and Theory," Soft Matter, **7**(14), pp. 6583–6589.

[12] Biot, M. A., 1963, "Surface Instability of Rubber in Compression," Appl. Sci. Res., **12**(2), pp. 168–182.